Design and thermal characterization of an induction-heated reactor for pyrolysis of solid waste

Oscar Sosa Sabogal [a,b,], Sylvie Valin [a], Sébastien Thiery [a], Sylvain Salvador [b]*

[a] *Univ. Grenoble Alpes, CEA, LITEN, DTBH, 17 rue des Martyrs, Grenoble Cedex 09, 38000 France*
[b] *Centre RAPSODEE, IMT Mines Albi, CNRS UMR 5302, Campus Jarlard, Albi Cedex 09, 81013, France*

ABSTRACT

Keywords:
Pyrolysis
Gasification
Solid waste
Fluidized bed reactor
Induction heating

A small-scale induction heated reactor (IHR) was specifically developed to study fast pyrolysis, here investigated as the first step of gasification process, representing some of the reaction conditions encountered in a fluidized bed reactor. First, the thermal response of the system was characterized at transient and steady state, and CFD calculations were performed to have a complete description of the temperature profiles inside the reactor. The novel device can handle a few grams of solid at temperatures up to 900 °C, allowing high heating rates (near 80 °C/s) and a uniform distribution of temperature in the sample. Secondly, the pyrolysis of a solid recovered fuel (SRF) sample was carried out at 800 °C, and the distribution and composition of reaction products were analyzed and compared with tests performed in a pilot scale fluidized bed reactor (FBR). The results obtained in the IHR showed a good reproducibility. The same main gas and tar species were measured in the IHR and FBR, with some differences in gas and tar composition that were attributed to the extent of secondary reactions, enhanced by higher heat transfer rates and the presence of bed material in the FBR.

1. Introduction

Solid waste that cannot be reused or recycled can be transformed through energy recovery processes, an interesting alternative to landfill. Waste derived fuels are produced from industrial or household waste, which include common materials with high calorific values like plastics, textiles, wood, and elastomers (Garcés et al., 2016). After incineration, pyrolysis and gasification are the most common valorization routes. Pyrolysis is a thermochemical process where the carbonaceous feedstock decomposes in absence of oxygen to produce permanent volatiles (gas), condensable hydrocarbons (tar) and often a solid residue (char). Gasification usually occurs at temperatures above 700 °C, in presence of an oxidizing agent that is fed below the stoichiometric amount needed for total oxidation.

The produced gas can be directly burnt to produce energy and heat or, after cleaning, used in a synthesis process to produce biofuels or chemicals. The yields of products and their composition highly depend on reactor design, process parameters, and feedstock characteristics. Among the available technologies in thermochemical conversion, fluidized bed reactors are widely used in the pyro-gasification of biomass and waste since they are suitable for heterogeneous streams (Benedikt et al., 2018). Compared to fixed bed reactors, they are characterized by higher mass and energy transfer rates, achieving higher conversion rates and low tar yields (Park et al., 2018).

Testing different feedstocks or conditions in a fluidized bed pilot can be costly in time and resources. Lab scale devices offer a simpler and more flexible solution, however, the reaction conditions found in an industrial fluidized bed reactor are difficult to scale down (Leion et al., 2018). The rate and extent of decomposition of the feedstock during the pyrolysis process, is mostly influenced by the undergone thermal history. This history is classically defined by three parameters: the heating rate, the final temperature, and the total residence time (Pasel and Wanzl, 2003). Slow heating rates induce high residence times and favor

char formation, while high heating rates and high temperatures favor gas products (Efika et al., 2018).

Most researchers have used thermogravimetric analysis (TGA) to study the pyrolysis of solid carbonaceous feedstocks and char gasification kinetics (Aluri et al., 2018; Porshnov et al., 2018; Zhou et al., 2015). In this technique, mass loss is continuously measured while the sample is subjected to a temperature treatment at a constant heating rate or a constant temperature under controlled atmosphere. However, conventional thermogravimetric analyzers present some limitations such as low heating rates (~1 °C/s) and limited gas-solid contact (Saadatkhah et al., 2020; Samih and Chaouki, 2015). Sample mass is around 10–100 mg, which makes it difficult to obtain representative results, especially for mixtures as heterogeneous as waste derived fuels (Robinson et al., 2016). Curie-point and wire mesh reactors achieve very high heating rates (>10⁴ °C/s), however sample mass is also in the scale of a few milligrams and reaction products are difficult to quantify (Zhu et al., 2020). Other devices use larger amounts of sample, like fixed bed reactors (Hwang et al., 2014), drop tube and boat furnaces (Daouk et al., 2018). Heat and mass transfer limitations may become significant if the heating rate is not high enough, if large particles are used or if there is not a good contact between the gas and the solid (Cortazar et al., 2020).

Some of the pyrolysis and gasification steps are endothermic, which means that enough heat must be provided to the reactor to sustain these reactions. In fluidized bed reactors, heat can be transferred from the bed material (heated in a separate vessel), from a hot fluidizing gas, by the oxidation of a feedstock fraction (autothermal operation) or by external means (Zhang et al., 2018). In lab scale installations heat is transferred to the reactor wall externally. Electric resistance heating is one of the most common sources at this scale. It offers a good temperature control; however, it usually takes long time to reach the setpoint temperature due to thermal inertia. High temperature differences appear between the reactor wall and the sample, therefore, a major response delay is observed (Latifi and Chaouki, 2015). Alternative sources that can provide faster and more uniform heating are worth considering.

Widely used in the treatment of metal materials, induction heating is a contactless method in which an AC power source is used to supply an alternating current to a coil, which is wrapped around the work piece. This current generates an electromagnetic field on the work piece and consequently heats it by two phenomena: creation of eddy currents and magnetic hysteresis (Latifi and Chaouki, 2015). Induction heating offers several key features like rapid heating rates, precise temperature control and high energy efficiency, which makes it an interesting energy source for the study of thermal conversion processes (Henkel, 2014; Mishra et al., 2019; Muley et al., 2015). Induction heating has been previously used in a few pyrolysis studies (Gauthier et al., 2013; Latifi et al., 2014; Muley et al., 2015; Tsai et al., 2009), mainly focused on the maximization of the oil fraction, which generally induces temperatures below 600 °C. Therefore, the literature regarding pyro-gasification studies using an induction reactor is very scarce.

The present work focuses on the design and thermal characterization of a new induction-heated reactor (IHR), for the study of the thermochemical conversion of solid waste. The characteristics and thermal behavior of the developed reactor are presented in detail. Preliminary pyrolysis experiments were carried out with solid recovered fuel (SRF) samples to validate the setup, and their results are also presented and compared with tests made in a fluidized bed reactor (FBR). Pyrolysis is here studied as the first step of gasification process, and the distribution and characterization of gas and tar products are the main interests.

2. Description of the experimental setup and procedure

2.1. Design requirements

The device developed in this work was designed to reach reaction thermal conditions close to those of a fluidized bed reactor, frequently used in biomass and waste gasification.

These characteristics include heating rates between 100 and 1000 °C/s (Nilsson et al., 2012), a temperature range between 750 and 900 °C, and good gas/solid heat and mass transfer conditions. Gas residence times inside the hot reactor are usually between 0.5 and 10 s for bubbling fluidized bed reactors, and between 0.5 and 1 s for circulating fluidized bed reactors (Marshall et al., 2014). For the present device, a residence time between 1 and 5 s was targeted, long enough to enable significant secondary reactions of volatiles (H_2, CO, CO_2, H_2O and hydrocarbons, including tar species). These reactions take place at temperatures above 600 °C before the volatiles exit the reactor freeboard zone (Barr et al., 2019).

The reactor was designed to handle a few grams of sample and to minimize heat and mass transfer limitations. A homogeneous temperature in the sample was desired along the whole reaction time. Temperature gradients within the reactor were reduced by preheating the carrier/gasification agent gas, before entering into contact with the sample. Finally, another objective was to collect all the reaction products (solids, condensable and permanent gases) for further analyses and quantification.

2.2. Detailed description of the setup

The designed and developed lab-scale setup is shown in Fig. 1. It consists of an induction-heated reactor, followed by a condensable and gas products collection system, and analysis modules.

The reactor consists of a stainless-steel tube of 560 mm in height, 31.75 mm in external diameter and with a thickness of 0.8 mm. The type of stainless steel used for the reactor was 316L; it can withstand temperatures up to 900 °C. A constant nitrogen flow fed from the bottom of the reactor is used to purge the system and to sweep the produced volatiles during the course of the experiment. Flowrate is set with a BROOKS's 5851S mass flowmeter controlled by a LabVIEW interface. A custom build heat exchanger helps to preheat the entering gas. The arrangement consists of two concentric metallic Inconel 600 tubes, with a height of 50 mm, a thickness of 0.5 mm and a diameter of 20 mm and 23 mm respectively. Entering gases are forced to pass through the small spaces (2 mm) between the reactor tube and the exchanger walls, for a total of 3 passes (Fig. 2).

The crucible consists in a metallic cylinder (of 27 mm in diameter and 55 cm in height), with the bottom part made of wire mesh, which enables the gas to flow through the sample particles. It can contain up to 10 g of sample, depending on the bulk density of the feedstock. A ceramic ring of 5 mm in height acts as a support and places the crucible at the middle of the reactor tube, just on top of the preheater. A metallic mesh cone of 35 mm height placed below the crucible acts as a diffuser (Fig. 2). Above the sample, an empty region of 320 mm high allows the gas phase reactions to take place during a few seconds.

The reactor is heated externally by an induction setup. The reactor tube is surrounded by a water-cooled copper coil inductor of 24 turns disposed in a parallel layout, for a total height of 420 mm. A generator (HFP 12, EFD induction Gmbh, 12 kW) supplies energy to the induction circuit. Maximal output value is limited to 75% by an internal setting. Setpoint temperature is adjusted with a GEFRAN 2500 PID controller, which is connected to a two-color optical pyrometer (Impac IGAR 6, range between 100 and 2000 °C, response time 2 ms).
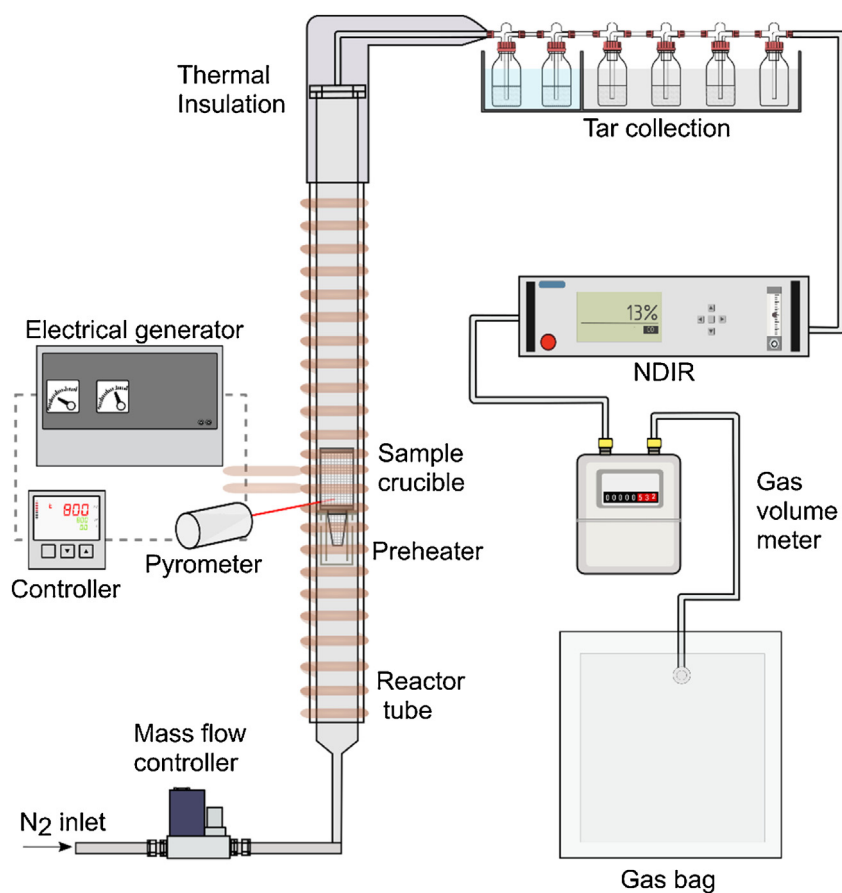
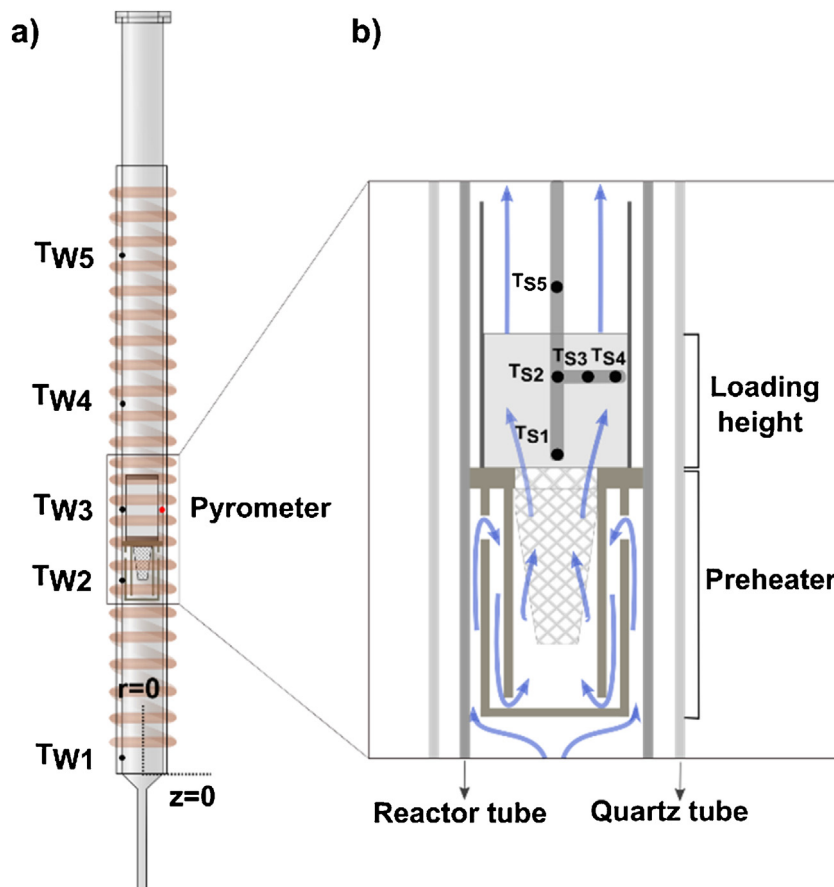**Fig. 1 – Experimental setup of the induction heated reactor (IHR).**

Fig. 2 – a) Schematic of the reactor tube outlining the wall thermal measuring elements position. **b)** Cross sectional illustration of the preheater and sample region, detailing the position of the sample thermocouples in the T shaped rod and the N_2 flow direction.

A quartz tube is placed to create a 5 mm gap between the coil and the reactor (5 mm gap).

2.2.1. Product collection and analysis modules

Product gas flows upwards and leaves the reactor through the outlet line, which goes to the condensable trapping system. The top portion and the outlet line are heated and insulated to keep temperature above 250 °C, to prevent tar and water condensation before reaching the traps. Five gas washing bottles filled with 2-propanol are used to collect condensable species (water and tar) present in the stream. Glass wool and glass beads are used to improve the contact between the gas and the solvent. The first two bottles are installed in an ice bath at 0 °C, while the other three are immersed in a carbonic ice and 2-propanol mixture at −70 °C. One empty bottle is placed at the end of the sampling train. Tar species are subsequently analyzed and quantified using a gas chromatograph with a flame ionization detector (GC-MS/FID, Agilent 7890A).

Non-condensable gases flow towards an online NDIR sensor (Non-Dispersive Infrared Detector), which record the CO, CO_2 and CH_4 concentrations every 1 s. Total volumetric flowrate of the produced gases is determined by a diaphragm gas meter placed at the outlet of the NDIR analyzer. Simultaneously, gases are collected in the Tedlar bag during the whole duration of the test (20 min). The test is finished when no gas concentration change is observed in NDIR. The gas from the bag is then accurately analyzed in the μGC. An Agilent 3000A chromatograph equipped with four columns is used. The species that can be quantified are O_2, CO_2, CO, CH_4, N_2, H_2, C_2H_2, C_2H_4, C_2H_6, C_3H_8, C_6H_6 (benzene), C_7H_8 (toluene), C_8H_{10} (xylene and ethylbenzene), H_2S, COS, and H_2O in vapor phase. Remaining solid products in the sample crucible are weighed and collected for further analyses once the reactor has cooled down to ambient temperature.

3. Reactor thermal characterization

It is common to assume that reaction temperature is that of the heating source, or that the temperature inside the reactor is uniform, although this can lead to major errors (Lédé, 2013). When using induction heating, the the position of the coil and of working frequency are crucial to attain a desired temperature profile for a specific workpiece (Hadad et al., 2016). For this setup, the space between the coils, uniform at first, was modified to concentrate the magnetic field density along the preheater and the sample zone, where the required power density was higher. The positions of the coil and that of the pyrometer spot were also varied, and the configuration leading to the shorter response time was kept.

Heating profiles inside and at the external surface of the reactor were monitored in various test runs at atmospheric pressure, without and in presence of an inert sample. The reactor was heated from ambient temperature to 800 °C (pyrometer temperature), and then held at stable conditions for several minutes to ensure that steady state was reached. Carrier gas (N_2) flowrate was set at 1 NL/min. Temperatures at the wall external surface were measured by five K type thermocouples (TW1 to TW5) of 0.5 mm in diameter, distributed on the outer surface at z = 10, 155, 207, 268, 375 mm as shown in Fig. 2. F AT shaped rod with five K type thermocouples (TS1 to TS5) at different radial (r = 0, 6, 13 mm) and axial positions (z = 185, 210, 235 mm) was introduced into the crucible as displayed in Fig. 2b.
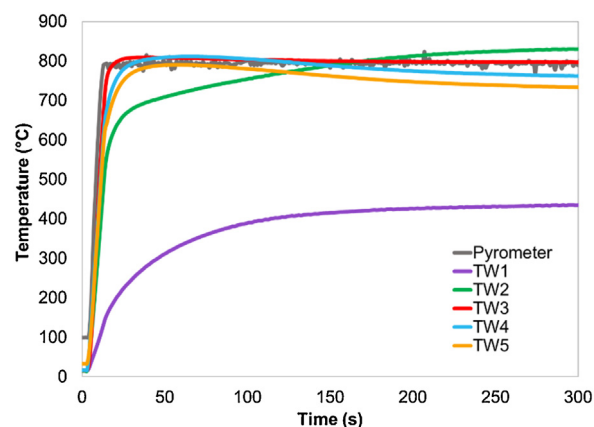

Fig. 3 – Temperature evolution at different locations along the reactor outer wall.

3.1. Dynamic temperature profiles

The evolution of temperatures at the external reactor tube surface is shown as a function of time in Fig. 3. Tw1 is the closest thermocouple to gas entrance and is placed outside the heated area, so its temperature was far below the setpoint. The wall temperature at the sample height (Tw3) reached the setpoint value in 15 s approximately, following a linear behavior with a steep slope of 80 °C/s. At the preheater position (Tw2), the thermal response was slower due to the inertia of the internal elements and to the colder gas flowing along the exchanger walls. Temperatures along the empty zone above the sample (Tw4, Tw5) were similar, reaching a peak temperature just above the setpoint after 60 s followed by a slight decrease before stabilizing around 750 °C.

The thermal profile inside the reactor was established for two cases and is shown in Fig. 4. In the first case, the crucible was empty, while in the second case it was filled with a bed of chemically inert material (alumina) with an average particle size of 4 mm. The loading height was about 30 mm. A significant temperature difference was observed between the reactor wall (pyrometer) and the T shaped rod thermocouples for both cases.

Differences between the internal thermocouples (TS1 to TS5) measurements were not significant for the empty case (Fig. 4a), which suggests a uniform temperature profile in both axial and radial directions. For the second case, the fastest response was recorded above the sample (TS5, z = 235 mm), where the thermocouple was subjected to radiant heat incident from the reactor wall and from the top particles of the bed. This explains why the temperature exceeded the setpoint value before reaching a stable value. At the middle of the bed (z = 210 mm) the temperature nearest to the hot reactor wall (TS4) increased faster than the one at the center (TS2), which was expected due to the thermal resistance of the bed material. The gradient in the radial direction was very low when compared with the thermal gradient in the axial direction. A similar result was observed in previous works of Fernández et al. (2016) and Chatterjee et al. (2017) where negligible radial temperature change was observed on two radio-frequency heated reactors with similar length to diameter ratios. In contrast, temperature differences in the axial direction reached several hundreds of °C. The slowest response was measured at the bottom of the crucible (TS1). In this point, carrier gas coming from the preheater meets the colder solid particles and then must flow through the empty spaces of the bed, which implies an additional thermal resistance.
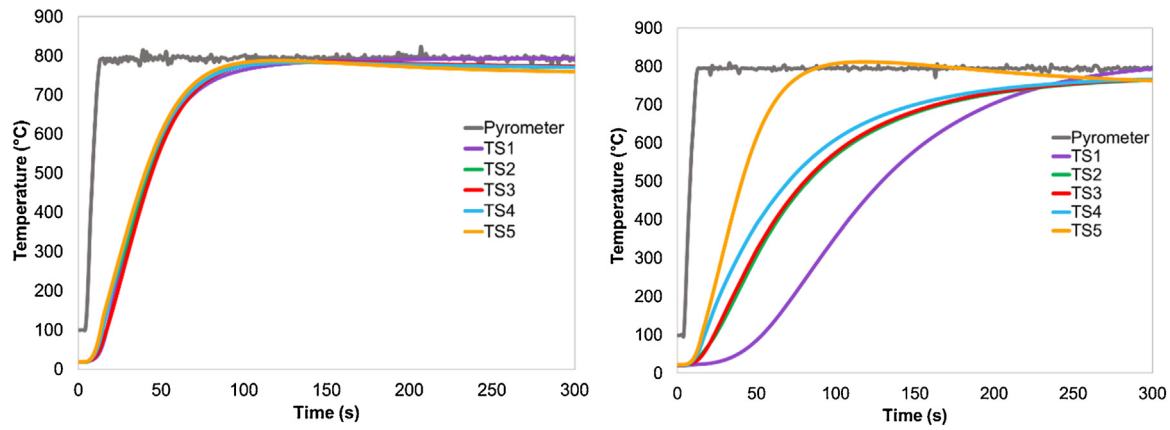
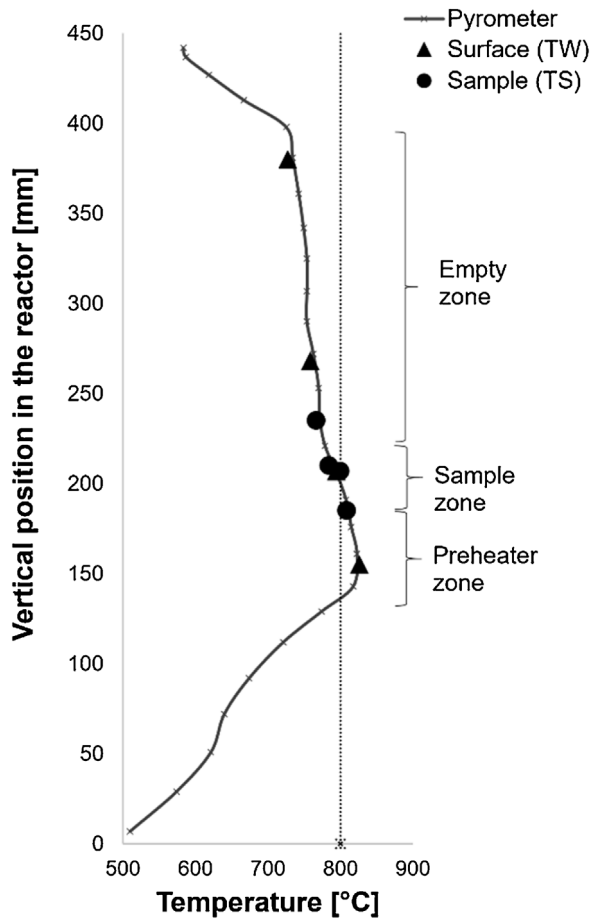**Fig. 4 – Temperature evolution a) in the empty crucible and b) in the crucible filled with ceramic material.**

Fig. 5 – Temperature distribution along the reactor wall at steady state for a setpoint of 800 °C.

Table 1 – Chemical composition of the feedstock.	
	SRF
Moisture (ar)	5.17%
Ash (db)	16.38%
C (db)	48%
H (db)	6%
O (db[a])	26.68%
N (db)	1.33%
S (db)	0.47%
Cl (db)	1.14%

ar: as received; db: dry basis.
[a] By difference.

For the conditions of this test, Reynolds number was equal to 11.75, which indicates a laminar flow regime inside the reactor. The main heat transfer mechanisms involved during the heating of the sample were radiation between the inner walls, and bed particles, followed by a smaller contribution of convection, due to the low gas flowrate. It took about 300 s for the thermocouples of the inner bed to reach their endpoint value, compared to only 100 s for the empty crucible case.

The time needed to reach the setpoint temperature depends on the thermal properties of the elements inside the reactor. Thermal diffusivity ($\alpha = k/\rho\, C_p$)] is an indicator of how fast a material respond to a temperature change. Thermal diffusivity increases with temperature for nitrogen gas, while the behavior is the opposite for alumina. At 800 °C, α is equal to 180,8 mm^2/s for nitrogen gas and 2.22 mm^2/s for alumina, which is consistent with the responses observed for the two case studies in Fig. 4.

Thermal properties for a solid fuel will depend on its composition, and its heating behavior will be influenced the by the changes it is subjected to during its pyrolysis. In the case of lignocellulosic materials like wood, some part of the feedstock will be released as volatile matter and the rest will remain as char. Redko et al. (2020) found that the effective diffusivity at 600 °C of raw wood (0.03 mm^2/s) was significantly lower compared to that of its char (0.5 mm^2/s), and that char diffusivity tended to increase with temperature. For other waste materials like plastics, devolatilization occurs between 400 and 500 °C in a single step without char formation, with the exception of PVC (Ranzi et al., 2016). Gases produced from plastic pyrolysis present diffusivities in the range of 8–70 mm^2/s at high temperatures depending on the monomer (Honus et al., 2018). The temperature evolution of a solid waste sample will be intermediate between the two cases, first it will behave as the solid, and then once its devolatilization is complete, it will behave as in the case of gas.

3.2. Steady state conditions

A second two-color optical pyrometer (Impac IGAR 12-LO, 350−1300 °C range) placed on a moving support was used to measure the temperature profile along the reactor external surface in steady state conditions. Both runs (with and without ceramic particle bed) showed the same result, so the mean temperature distribution for the two runs is shown in Fig. 5.

The maximum temperature reached inside the sample bulk (located between 180 and 210 mm) is 808 °C. Tempera-

ture discrepancies were under 10 °C in the bed (TS1 to TS4), which shows that the temperature is uniform and close to the setpoint temperature once the steady state is reached. The highest wall temperature (TW2 = 825 °C) was measured at 155 mm, where the preheater device is placed. Above the sample, an isothermal zone of about 200 mm long was maintained at 750 °C. This empty zone is analog to the freeboard zone in a fluidized bed reactor. The temperature progressively decreases above this point since the current density is much lower outside the coil.

3.3. Reactor modeling

Thermocouple reading inside the tubular reactor can be affected by the radiative heat transfer between the thermocouple and the surrounding walls. The thermocouple thus sees surrounding surfaces at a higher or lower temperature than the real gas temperature. To complete the description of the gas temperature inside the reactor, a finite element thermal modelling was performed at steady state. The commercial software ANSYS FLUENT R19.3 was used to perform these calculations.

Reactor geometry was discretized using a 2D-axysymmetric approach, including the exchanger and the sample holder. The model assumed that gas phase consisted solely of nitrogen, and a carrier gas flow rate was set as inlet boundary condition. Various carrier gas flowrates (0.5 and 4 L/min) were tested to see the preheater performance and the influence of the gas velocity in the temperature profile of the reactor. The solid bed of particles was considered by using the porous media zone condition, which was applied to a specific flow domain created for the zone inside the crucible.

Properties of gas and solid phases were calculated using temperature dependent functions. Atmospheric pressure was defined as the outlet condition. The experimental profile measured previously at the tube surface was implemented to describe the stationary wall temperature. Reactor walls were modeled using no-slip boundary condition for the gas phase. Based on the assumptions listed above, governing equations (mass, energy, and momentum) were solved numerically by a finite volume method. The PRESTO (PREssure STaggering Option) was used as the pressure interpolation scheme, recommended for problems involving flow through porous media. The discreet ordinates radiation model was used to model the radiation heat transfer. The convergence was verified by monitoring residuals and the mass and energy balances.

Fig. 6 shows the temperature distribution of the gas phase inside the reactor at steady state conditions for increasing gas flowrates. At the lowest values, inlet gas was properly heated by the heat exchanger, so its temperature remained above 790 °C in the crucible zone with a rather homogeneous profile in both axial and radial directions. As the N_2 flowrates increased, more pronounced temperature gradients were observed in the crucible zone, especially in the radial direction. Because of enhanced convection, the length of the isothermal empty zone above the crucible increased and the maximum temperature position shifted in the direction of the N_2 flowrate, as observed in the work of Chatterjee et al. (2017).

N_2 flowrates of 0.5 and 1 L/min are best suited to achieve a homogeneous temperature profile in the sample as desired. Under these conditions, the estimated residence time of the gas in the hot empty zone (temperatures between 750 °C and 800 °C) is between 2 and 4 s. These conditions were selected for the pyrolysis test presented in the next section.

4. Pyrolysis tests

Preliminary pyrolysis experiments were carried out with solid recovered fuel (SRF) samples to validate the whole setup operation and experimental procedure. Their results are presented in the present section and compared with tests made in a pilot scale bubbling fluidized bed reactor (FBR).

4.1. Feedstock

The SRF used for the pyrolysis experiments, was produced from industrial and household waste. The fuel, in the form of pellets of 1 cm in height and 5 mm in diameter, was characterized by ultimate and proximate analyses. Moisture content was determined at 105 °C while ash content was measured at 815 °C according to the ISO 1171standard. Elemental composition (C, H, N, S) was determined with an ELEMENTAR analyzer. Feedstock composition is listed in Table 1.

4.2. Test procedure

The crucible was filled with 2.3 g of dried SRF pellets (24 h at 105 °C) and placed in the reactor. Gas washing bottles were placed in the cooling baths and then connected to the reactor outlet. Nitrogen gas (0.5 L/min) was used to flush the entire system before the test and to carry the produced volatiles. Reactor was heated up to 800 °C and then held at this temperature for about 20 min. All the permanent gases were collected in a Tedlar bag, during the whole test and for an additional 20 min to ensure all the released products were collected. The gas meter reading and the composition of permanent gases as determined using micro GC were used to calculate the molar amounts of permanent gases. Liquid in the washing bottles was sampled and then analyzed by GC-MS/FID. Sample holder was weighed before and after the test to determine the char yield. The carbon conversion was defined as the ratio between the mass fraction of carbon in each product and the carbon content in the feedstock. Two tests were performed under the same conditions and the average values are presented. The values did not differ by more than 2%.

4.3. Product yields

The carbon distribution into each of the pyrolysis main products (permanent gases, tar, char) was determined and is presented in Fig. 7. The tar fraction is defined here as all condensable organic compounds with a higher molecular weight than toluene. The results of the present study (named here IHR for "Induction Heating Reactor") were compared with the ones obtained in the work of Valin et al. (2019) in which pyrolysis tests of the same batch of SRF were conducted at 800 °C in a pilot scale bubbling fluidized bed reactor (FBR) filled with olivine as bed material.

In both cases, most of the initial carbon was converted to gas products. A higher fraction of carbon remained in the char after pyrolysis in the IHR reactor compared with the FBR. This is consistent with the results obtained by Efika et al. (2015), where RDF samples were pyrolyzed at different heating rates in a horizontal tubular reactor. Indeed, higher heating rates are encountered in fluidized beds thanks to contact between
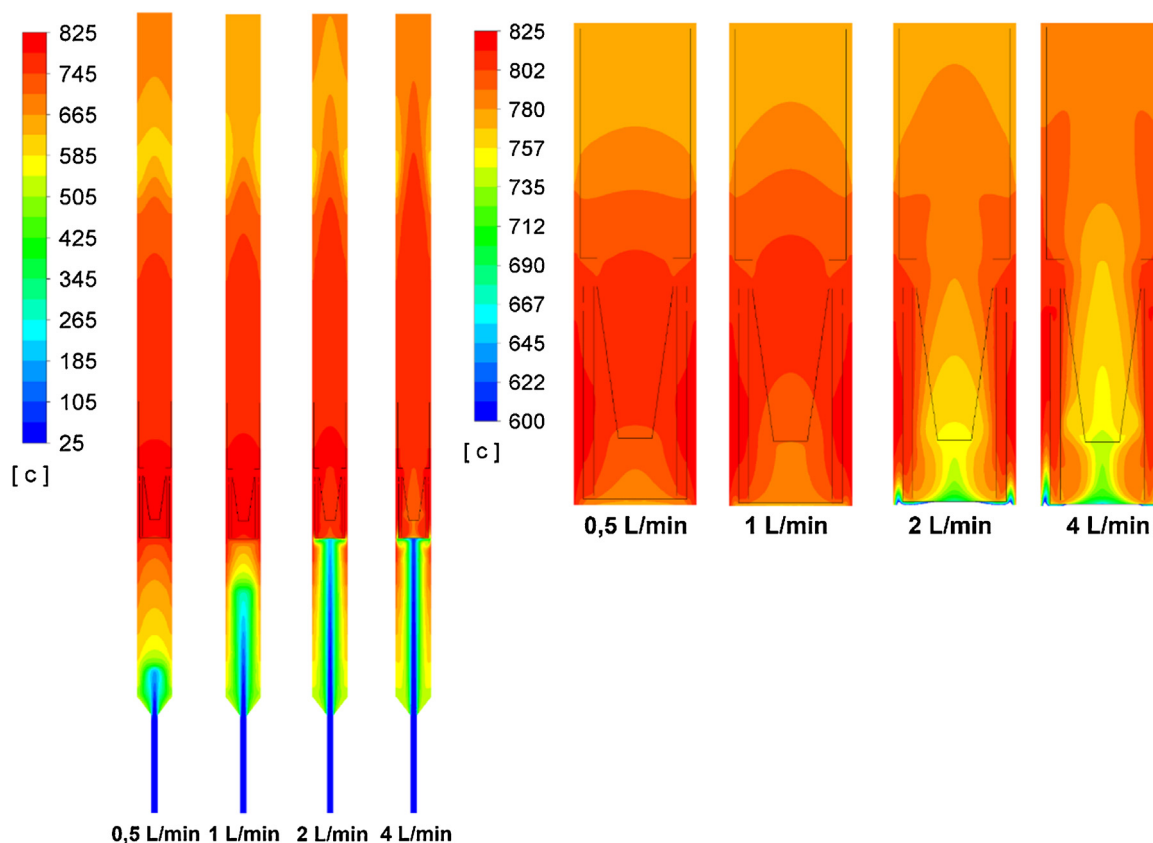
Fig. 6 – Contour plots of temperature distribution in the gas phase for different gas flowrates (left). Close up at the exchanger and sample zone (right).
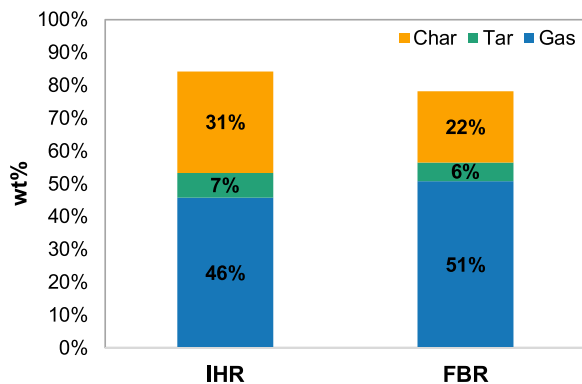

Fig. 7 – Carbon distribution into products obtained from RDF pyrolysis at 800 °C in the induction heating reactor and a pilot fluidized bed reactor.

Fig. 8 – Yield of non-condensable gases from RDF pyrolysis at 800 °C for the developed device and a pilot fluidized bed reactor.

hot bed material particles, gas, and feedstock particles, which favors the carbon conversion to volatiles. In addition to the heating rate, the higher temperature and residence time also contribute to the cracking of the primary vapors into light molecular weight hydrocarbons, leading to increased gas yield and lower tar yield. Carbon mass balance closure reached about 85 wt% in the IHR reactor and was slightly lower for the FBR (78%). The missing carbon fraction could be attributed to condensable products that are deposited in the reactor outlet despite of tracing, and to hydrocarbons that cannot be identified or quantified in the GC-MS/FID analysis.

4.4. Gas products

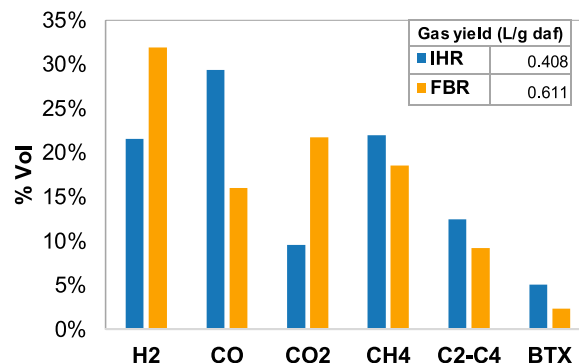Produced gas yield and its volumetric composition are compared in Fig. 8 for both setups. In this study, gas species included H_2, CO_2, CO, CH_4, light hydrocarbons from two to four carbon atoms (C_2H_2, C_2H_4, C_2H_6, C_3H_8, C_3H_6, C_4H_6-butadiene) and light aromatic species like C_6H_6 (benzene) and C_7H_8 (toluene), grouped and named here BTX.

As stated before, total gas production was higher in the FBR reactor. For the IHR reactor, CO was the most abundant gas (29.4%), followed by methane (22%) and hydrogen (21.5%). The fluidized bed gas presented higher concentrations of H_2 (31.9%) and CO_2 (21.7%) compared to the IHR gas. This could be due to higher residence time as well as the presence of bed material in the FBR, which favored hydrocarbon break-down reactions resulting in more H_2. Olivine bed improves the reforming of phenol and other tars, as seen in the work of Nitsch et al. (2013). The contents of methane, light hydrocarbons and BTX were slightly lower in the FBR. A similar trend was observed by Pasel and Wanzl (2003), who compared the
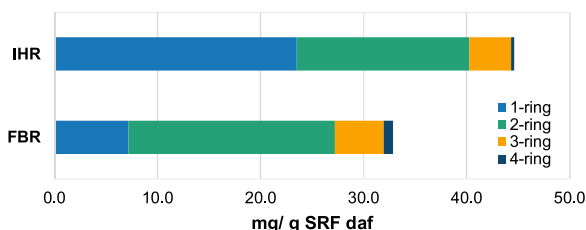
Fig. 9 – Composition of tar produced from the pyrolysis of SRF in the developed device and a pilot fluidized bed reactor.

benzene yield from shredded waste pyrolysis in various types of equipment, including a tubular and a fluidizing reactor.

4.5. Tar products

The condensable fraction recovered in the gas washing bottles contains numerous organic species, which were then analyzed and quantified by GC-MS/FID. Here, the main tar species from pyrolysis in both reactors are shown in Fig. 9. Composition of tar produced from the pyrolysis of SRF in the developed device and a pilot fluidized bed reactor. Fig. 9, and are classified in four groups based on the number of aromatic rings in their structure.

Longer residence times and the presence of bed material possibly favored the extent of secondary reactions in the fluidized bed reactor, which decreased the total amount of tar when compared to the IHR. Most of the tar species generated in the IHR reactor were in the first group, consisting mostly of styrene (74%), and followed by indene and phenol. In the case of the fluidized bed, naphthalene, with two rings, was the most abundant component (70%). Heavier polycyclic aromatic hydrocarbons (PAHs) such as anthracene and pyrene (3 and 4 rings) were present in the tar from the FBR, while their amount for the IHR case was negligible. High temperatures (above 700 °C) promote the appearance of PAHs, as a product of aromatization and rearrangement reactions of aliphatic and monocyclic compounds (Pasel and Wanzl, 2003).

5. Conclusions

An induction-heated reactor was developed to perform pyrolysis experiments of waste derived fuels and its constituent materials. Some of the features of the developed device included a gas preheating system, high heating rates and the possibility of recovering and analyzing all reaction products. Experimental and CFD results provided a complete description of the temperature profiles for the surface, the sample and the gas inside the reactor. Heat provided by the induction circuit enabled to maintain a uniform temperature inside the sample carrier gas flowrates between 0.5 and 1 NL/min.

The IHR was used to perform the pyrolysis of a SRF sample and the results were compared with tests made in a pilot scale fluidized bed reactor. Reaction conditions in the IHR reactor were close to intermediate to fast pyrolysis (heating rate 75 °C/s, volatiles residence time ≈ 4 s). Char yield indicates that the heating rate in the solid sample is lower in the IHR compared to the FBR.

Main permanent gas products were similar for the two reactors; however, residence time and the presence of the bed material had an influence on the extent of secondary reactions, which modified the distribution of the permanent gas species and tar products. In the future, experiments will be performed with raw materials used as model constitutents of wastes (such as plastic polymers, woody biomass, paper or cardboard), and their mixtures. Results obtained in the IHR reactor, carried out under controlled and well characterized conditions, will then be useful for the development and improvement of prediction models of the reaction products, and thus contribute to the understanding of pyrolysis and gasification at various scales.

Declaration of competing interest

The authors declare that they have no known competing commercial interests or personal relationships that could have appeared to influence the work reported in this paper.

References

Aluri, S., Syed, A., Flick, D.W., Muzzy, J.D., Sievers, C., Agrawal, P.K., 2018. Pyrolysis and gasification studies of model refuse derived fuel (RDF) using thermogravimetric analysis. Fuel Process. Technol. 179 (Oct), 154–166, http://dx.doi.org/10.1016/j.fuproc.2018.06.010.

Barr, M.R., Volpe, R., Kandiyoti, R., 2019. Influence of reactor design on product distributions from biomass pyrolysis. ACS Sustain. Chem. Eng. 7 (Aug (16)), 13734–13745, http://dx.doi.org/10.1021/acssuschemeng.9b01368.

Benedikt, F., Schmid, J.C., Fuchs, J., Mauerhofer, A.M., Müller, S., Hofbauer, H., 2018. Fuel flexible gasification with an advanced 100 kW dual fluidized bed steam gasification pilot plant. Energy 164 (Dec), 329–343, http://dx.doi.org/10.1016/j.energy.2018.08.146.

Chatterjee, S., Houlding, T.K., Doluda, V.Yu., Molchanov, V.P., Matveeva, V.G., Rebrov, E.V., 2017. Thermal behavior of a catalytic packed-bed milli-reactor operated under radio frequency heating. Ind. Eng. Chem. Res. 56 (Nov (45)), 13273–13280, http://dx.doi.org/10.1021/acs.iecr.7b01723.

Cortazar, M., Lopez, G., Alvarez, J., Arregi, A., Amutio, M., Bilbao, J., Olazar, M., 2020. Experimental study and modeling of biomass char gasification kinetics in a novel thermogravimetric flow reactor. Chem. Eng. J. 396 (Sep), 125200, http://dx.doi.org/10.1016/j.cej.2020.125200.

Daouk, E., Sani, R., Pham Minh, D., Nzihou, A., 2018. Thermo-conversion of Solid Recovered Fuels under inert and oxidative atmospheres: gas composition and chlorine distribution. Fuel 225 (Aug), 54–61, http://dx.doi.org/10.1016/j.fuel.2018.03.136.

Efika, E.C., Onwudili, J.A., Williams, P.T., 2015. Products from the high temperature pyrolysis of RDF at slow and rapid heating rates. J. Anal. Appl. Pyrolysis 112 (Mar), 14–22, http://dx.doi.org/10.1016/j.jaap.2015.01.004.

Efika, C.E., Onwudili, J.A., Williams, P.T., 2018. Influence of heating rates on the products of high-temperature pyrolysis of waste wood pellets and biomass model compounds. Waste Manag. 76 (Jun), 497–506, http://dx.doi.org/10.1016/j.wasman.2018.03.021.

Fernández, J., Sotenko, M., Derevschikov, V., Lysikov, A., Rebrov, E.V., 2016. A radiofrequency heated reactor system for post-combustion carbon capture. Chem. Eng. Process. Process Intensif. 108 (Oct), 17–26, http://dx.doi.org/10.1016/j.cep.2016.07.004.

Garcés, D., Díaz, E., Sastre, H., Ordóñez, S., González-LaFuente, J.M., 2016. Evaluation of the potential of different high calorific waste fractions for the preparation of solid recovered fuels. Waste Manag. 47 (Jan), 164–173, http://dx.doi.org/10.1016/j.wasman.2015.08.029.

Gauthier, G., Melkior, T., Grateau, M., Thiery, S., Salvador, S., 2013. Pyrolysis of centimetre-scale wood particles: new experimental developments and results. J. Anal. Appl. Pyrolysis 104 (Nov), 521–530, http://dx.doi.org/10.1016/j.jaap.2013.05.017.

Hadad, Y., Kochavi, E., Levy, A., 2016. Inductive heating with a stepped diameter crucible. Appl. Therm. Eng. 102 (Jun), 149–157, http://dx.doi.org/10.1016/j.applthermaleng.2016.03.151.

Henkel, C., 2014. A study of induction pyrolysis of lignicellulosic biomass for the production of bio-oil. LSU Masters Theses (Jan) [Online]. Available: https://digitalcommons.lsu.edu/gradschool_theses/447.

Honus, S., Kumagai, S., Fedorko, G., Molnár, V., Yoshioka, T., 2018. Pyrolysis gases produced from individual and mixed PE, PP, PS, PVC, and PET—part I: production and physical properties. Fuel 221 (Jun), 346–360, http://dx.doi.org/10.1016/j.fuel.2018.02.074.

Hwang, I.-H., Kobayashi, J., Kawamoto, K., 2014. Characterization of products obtained from pyrolysis and steam gasification of wood waste, RDF, and RPF. Waste Manag. 34 (Feb (2)), 402–410, http://dx.doi.org/10.1016/j.wasman.2013.10.009.

Latifi, M., Chaouki, J., 2015. A novel induction heating fluidized bed reactor: its design and applications in high temperature screening tests with solid feedstocks and prediction of defluidization state. AIChE J. 61 (5), 1507–1523, http://dx.doi.org/10.1002/aic.14749.

Latifi, M., Berruti, F., Briens, C., 2014. Non-catalytic and catalytic steam reforming of a bio-oil model compound in a novel 'Jiggle Bed' reactor. Fuel 129 (Aug), 278–291, http://dx.doi.org/10.1016/j.fuel.2014.03.053.

Lédé, J., 2013. Biomass fast pyrolysis reactors: a review of a few scientific challenges and of related recommended research topics. Oil Gas Sci. Technol. – Rev. D'IFP Energ. Nouv. 68 (Sep (5)), 801–814, http://dx.doi.org/10.2516/ogst/2013108.

Leion, H., Frick, V., Hildor, F., 2018. Experimental method and setup for laboratory fluidized bed reactor testing. Energies 11 (Oct (10)), 2505, http://dx.doi.org/10.3390/en11102505.

Marshall, A.J., Wu, P.F., Mun, S.-H., Lalonde, C., 2014. Commercial application of pyrolysis technology in agriculture. Am. Soc. Agric. Biol. Eng. Annu. Int. Meet. 2014 ASABE 2014 5, 3868–3886.

Mishra, H., Patidar, B., Pante, A.S., Sharma, A., 2019. Mathematical modelling, simulation and experimental validation of resistance heating and induction heating techniques for E-waste treatment. IET Electr. Power Appl. 13 (4), 487–493, http://dx.doi.org/10.1049/iet-epa.2018.5535.

Muley, P.D., Henkel, C., Abdollahi, K.K., Boldor, D., 2015. Pyrolysis and catalytic upgrading of pinewood sawdust using an induction heating reactor. Energy Fuels 29 (Nov (11)), 7375–7738, http://dx.doi.org/10.1021/acs.energyfuels.5b01878.

Nilsson, S., Gómez-Barea, A., Cano, D.F., 2012. Gasification reactivity of char from dried sewage sludge in a fluidized bed. Fuel 92 (Feb (1)), 346–353, http://dx.doi.org/10.1016/j.fuel.2011.07.031.

Nitsch, X., Commandré, J.-M., Clavel, P., Martin, E., Valette, J., Volle, G., 2013. Conversion of phenol-based tars over olivine and sand in a biomass gasification atmosphere. Energy Fuels 27 (Sep (9)), 5459–5465, http://dx.doi.org/10.1021/ef400817z.

Park, S.-W., Lee, J.-S., Yang, W.-S., Alam, M.T., Seo, Y.-C., 2018. A comparative study of the gasification of solid refuse fuel in downdraft fixed bed and bubbling fluidized bed reactors. Waste Biomass Valorization (Aug), http://dx.doi.org/10.1007/s12649-018-0431-6.

Pasel, C., Wanzl, W., 2003. Experimental investigations on reactor scale-up and optimisation of product quality in pyrolysis of shredder waste. Fuel Process. Technol. 80 (Jan (1)), 47–67, http://dx.doi.org/10.1016/S0378-3820(02)00187-X.

Porshnov, D., Ozols, V., Ansone-Bertina, L., Burlakovs, J., Klavins, M., 2018. Thermal decomposition study of major refuse derived fuel components. Energy Procedia 147 (Aug), 48–53, http://dx.doi.org/10.1016/j.egypro.2018.07.032.

Ranzi, E., Faravelli, T., Manenti, F., 2016. Pyrolysis, gasification, and combustion of solid fuels. Advances in Chemical Engineering, vol. 49. Elsevier, pp. 1–94.

Redko, T., Volford, A., Marek, E.J., Scott, S.A., Hayhurst, A.N., 2020. Measurement of the times for pyrolysis and the thermal diffusivity of a pyrolysing particle of wood and also of the resulting char. Combust. Flame 212 (Feb), 510–518, http://dx.doi.org/10.1016/j.combustflame.2019.10.024.

Robinson, T., Bronson, B., Gogolek, P., Mehrani, P., 2016. Sample preparation for thermo-gravimetric determination and thermo-gravimetric characterization of refuse derived fuel. Waste Manag. 48 (Feb), 265–274, http://dx.doi.org/10.1016/j.wasman.2015.11.018.

Saadatkhah, N., Garcia, A.C., Ackermann, S., Leclerc, P., Latifi, M., Samih, S., Patience, G.S., Chaouki, J., 2020. Experimental methods in chemical engineering: thermogravimetric analysis—TGA. Can. J. Chem. Eng. 98 (1), 34–43, http://dx.doi.org/10.1002/cjce.23673.

Samih, S., Chaouki, J., 2015. Development of a fluidized bed thermogravimetric analyzer. AIChE J. 61 (1), 84–89, http://dx.doi.org/10.1002/aic.14637.

Tsai, W.-T., Chang, J.-H., Hsien, K.-J., Chang, Y.-M., 2009. Production of pyrolytic liquids from industrial sewage sludges in an induction-heating reactor. Bioresour. Technol. 100 (Jan (1)), 406–412, http://dx.doi.org/10.1016/j.biortech.2008.06.013.

Valin, S., Ravel, S., Pons de Vincent, P., Thiery, S., Miller, H., 2019. Fluidized bed air gasification of solid recovered fuel and woody biomass: influence of experimental conditions on product gas and pollutant release. Fuel 242 (Apr), 664–672, http://dx.doi.org/10.1016/j.fuel.2019.01.094.

Zhang, L., Bao, Z., Xia, S., Lu, Q., Walters, K., 2018. Catalytic pyrolysis of biomass and polymer wastes. Catalysts 8 (Dec (12)), 659, http://dx.doi.org/10.3390/catal8120659.

Zhou, H., Long, Y., Meng, A., Li, Q., Zhang, Y., 2015. Thermogravimetric characteristics of typical municipal solid waste fractions during co-pyrolysis. Waste Manag. 38 (Apr), 194–200, http://dx.doi.org/10.1016/j.wasman.2014.09.027.

Zhu, J., Jin, L., Luo, Y., Hu, H., Xiong, Y., Wei, B., Wang, D., 2020. Fast co-pyrolysis of a massive Naomaohu coal and cedar mixture using rapid infrared heating. Energy Convers. Manage. 205 (Feb), 112442, http://dx.doi.org/10.1016/j.enconman.2019.112442.